



Controlled release of hydrogen by implantation of magnesium induces P53-mediated tumor cells apoptosis

Rui Zan^{a,b,1}, Hao Wang^{c,1}, Weijie Cai^{d,1}, Jiahua Ni^{a,***}, Bérengère J. C. Luthringer-Feyerabend^b, Wenhui Wang^a, Hongzhou Peng^a, Weiping Ji^d, Jun Yan^e, Jiazeng Xia^{c,**}, Yang Song^{a,****}, Xiaonong Zhang^{a,f,*}

^a State Key Laboratory of Metal Matrix Composites, School of Materials Science and Engineering, Shanghai Jiao Tong University, Shanghai, 200240, China

^b Institute of Metallic Biomaterials, Department of Biological Characterisation, Helmholtz-Zentrum Geesthacht (HZG), Geesthacht, 21502, Germany

^c Department of General Surgery and Translational Medicine Center, Wuxi No.2 People's Hospital, Affiliated Wuxi Clinical College of Nantong University, Jiangsu, 214002, China

^d Orthopaedic Department, Shanghai Jiao Tong University Affiliated Sixth People's Hospital, Shanghai, 200233, China

^e Department of General Surgery, Shanghai Jiao Tong University Affiliated Sixth People's Hospital, Shanghai, 200233, China

^f Suzhou Origin Medical Technology Co. Ltd., Suzhou, 215513, China

ARTICLE INFO

Keywords:

Biodegradable magnesium
Hydrogen
Tumor apoptosis
Underlying mechanism
P53

ABSTRACT

Hydrogen has been used to suppress tumor growth with considerable efficacy. Inhalation of hydrogen gas and oral ingestion of hydrogen-rich saline are two common systemic routes of hydrogen administration. We have developed a topical delivery method of hydrogen at targeted sites through the degradation of magnesium-based biomaterials. However, the underlying mechanism of hydrogen's role in cancer treatment remains ambiguous. Here, we investigate the mechanism of tumor cell apoptosis triggered by the hydrogen released from magnesium-based biomaterials. We find that the localized release of hydrogen increases the expression level of P53 tumor suppressor proteins, as demonstrated by the *in vitro* RNA sequencing and protein expression analysis. Then, the P53 proteins disrupt the membrane potential of mitochondria, activate autophagy, suppress the reactive oxygen species in cancer cells, and finally result in tumor suppression. The anti-tumor efficacy of magnesium-based biomaterials is further validated *in vivo* by inserting magnesium wire into the subcutaneous tumor in a mouse. We also discovered that the minimal hydrogen concentration from magnesium wires to trigger substantial tumor apoptosis is 91.2 $\mu\text{L}/\text{mm}^3$ per day, which is much lower than that required for hydrogen inhalation. Taken together, these findings reveal the release of H_2 from magnesium-based biomaterial exerts its anti-tumoral activity by activating the P53-mediated lysosome-mitochondria apoptosis signaling pathway, which strengthens the therapeutic potential of this biomaterial as localized anti-tumor treatment.

1. Introduction

Hydrogen gas (H_2) serves as a therapeutic medical gas in the treatment of inflammation [1,2], brain injury [3], and Alzheimer's disease [4]. The mechanism of therapeutic action is often attributed to the H_2 -mediated reduction of highly cytotoxic reactive oxygen species

(ROS), including peroxynitrite (ONOO^-) and hydroxyl radical ($\bullet\text{OH}$) without disturbing signaling of normal cells [5]. Since the first report of the anti-tumor property of H_2 in 1975, molecular H_2 has been extensively studied as a new therapeutic agent [6]. Molecular H_2 induces apoptosis of tumor cells and thereby suppresses the formation and growth of tumors [7–10]. H_2 also improves outcomes of conventional

Peer review under responsibility of KeAi Communications Co., Ltd.

* Corresponding author. State Key Laboratory of Metal Matrix Composites, School of Materials Science and Engineering, Shanghai Jiao Tong University, Shanghai, 200240, China.

** Corresponding author.

*** Corresponding author.

**** Corresponding author.

E-mail addresses: nijiahua2012@gmail.com (J. Ni), xjz_wuxi@alumni.sjtu.edu.cn (J. Xia), nanosurface@sjtu.edu.cn (Y. Song), xnzhang@sjtu.edu.cn (X. Zhang).

¹ Authors contributed equally to this work.

<https://doi.org/10.1016/j.bioactmat.2021.07.026>

Received 16 May 2021; Received in revised form 3 July 2021; Accepted 21 July 2021

Available online 9 August 2021

2452-199X/© 2021 The Authors. Publishing services by Elsevier B.V. on behalf of KeAi Communications Co. Ltd. This is an open access article under the CC

BY-NC-ND license (<http://creativecommons.org/licenses/by-nc-nd/4.0/>).

tumor treatment such as photothermal therapy and chemotherapy [11, 12]. Clinically, H₂ gas has been used to improve the prognosis in patients with stage IV colorectal cancer [13].

Common routes of H₂ administration include inhalation of hydrogen-containing air [14], injection of hydrogen-rich saline [15], and oral uptake of hydrogen-rich water [16]. Unfortunately, these H₂-delivery approaches often have limited therapeutic efficacy against tumors, as achieving hydrogen saturation in body fluids around the tumor is difficult. To overcome this challenge, new strategies to obtain a locally saturated H₂ environment and improve the efficacy of tumor-targeting is being exploited, such as generating microbubbles [17] or using nanoparticles of iron (Fe) [18], palladium hydride (PdH_{0.2}) [19], and magnesium diboride (MgB₂) [20] as H₂ carriers. However, the nondegradability and cytotoxicity of these nanoparticles also elevate health risks. A safer and more efficient H₂ administration approach is desired in clinical applications.

As a biodegradable metal, magnesium (Mg) spontaneously degrades into magnesium hydroxide and release hydrogen gas under physiological or buffer conditions due to its relatively low standard reduction potential ($-2.37V_{SHE}$) [21]. Controlled degradation of Mg biomaterial is safe and well-tolerated in animals and humans [22,23]. *In vivo* degradation of Mg biomaterials can create a gaseous H₂-rich environment as high as 1.46 mM near the implants [24], which surpasses the saturated concentration of hydrogen in water (0.8 mM). While the application of Mg to generate oversaturated H₂ for tumor and inflammation therapy has been reported [25–27], a mechanistic understanding on how hydrogen can trigger the apoptosis of tumor cells and the signaling pathway involved is missing.

In this study, we report the controlled release of hydrogen from biodegradable Mg by varying the pH value of the immersion solution and the specific surface area of Mg exposed to the immersion solution. Using a model of colon carcinoma treatment, we study the apoptosis rate of HCT116 cells after different levels of hydrogen exposition. Reactive oxygen species scavenging and expression of the tumor-suppressing genes were measured to identify the mechanism of anti-tumor action at different H₂ levels. The antitumor activity is ascribed to the upregulation of P53 tumor suppression protein, resulting in damages in the mitochondrial membrane, followed by activation of autophagy and suppression of reactive oxygen species. Our results indicate that the activation of tumor cell apoptosis requires a minimum inhibitory concentration of hydrogen around 91.2 $\mu\text{L}/\text{d}/\text{mm}^3$. This provides a primary guide for anti-tumor therapy in clinical applications.

2. Materials and methods

2.1. Material processing and microstructural analysis

Mg sheets (purity: 99.98 wt%, size: 12 × 10 × 0.4 mm) and Mg wires (purity: 99.98 wt%, size: \varnothing 1 × 5 mm) used in this work were supplied by Suzhou Origin Medical Technology Co. Ltd., China. Mg sheets were ground with 800# SiC abrasive paper from both sides and subsequently cleaned for 10 min with acetone and 10 min with 100 % ethanol in an ultrasonic bath. After cleaning, Mg samples were immersed into 70 % ethanol for 15 min and transfer to a clean bench for 15min with ultraviolet (UV) irradiation.

2.2. Electrochemical test

Electrochemical measurements were carried out using an electrochemical workstation (Chenhua, CHI660E, China). The potentiodynamic polarization tests were performed by applying an open-circuit potential (OCP) from -500 mV to $+500$ mV at a scan rate of 2 mV/s. The exposed area of the high purity Mg (HP-Mg) sheet was 1.2 cm², which serve as the working electrode. The electrolyte solution was phosphate buffered saline (PBS, Gibco, USA) solution supplemented with N-2-hydroxyethylpiperazine-N-2-ethane sulfonic acid (HEPES, Aladdin,

China) buffer, and the pH values of the electrolyte solution were 5.6, 6.5, and 7.4, separately.

2.3. Measurement of H₂ evolution from Mg

HP-Mg sheets were immersed in 10 mL PBS solution with different pH values (pH = 7.4, 6.5, 5.6), and the released H₂ was collected through an inverted funnel and its total volume was numerated through a calibrated burette, which was described in detail in previous work [28]. The real-time concentration of H₂ dissolved in PBS was measured by a dissolved hydrogen analyzer (Truslex, ENH-1000, Japan). In a separate experiment, the exposed surface area of Mg sheets was varied from 1.2 to 4.8 cm², and the total volume of released hydrogen and the real-time concentration of dissolved hydrogen in PBS were recorded.

In animal experiments, the total volume of H₂ released from Mg was calculated by monitoring the volume loss of Mg wires. A micro-CT scanner (Scanco Medical, μCT 100, Swiss) was used to scan Mg wire and quantify the volume of remaining Mg before and on the 8th days, 16th days, and 24th days after implantation (n = 3).

2.4. Design of H₂-emitting devices

An H₂-emitting device [29,30] was designed into three layers, as shown in Fig. 2b: a bottom layer of the standard six-well microplate, a gasket plate made of polypropylene in the middle, and a top layer of transwell chamber. Each microwell was filled with two pieces of Mg sheets and 2 mL of PBS solutions. The pH value of the PBS solution was adjusted by adding HEPES until the final pH reaches 7.4, 6.5, and 5.6. A control group was set without any H₂ release. All transwell chambers were coated with air-permeable polycarbonate membranes (0.4 μm pore size), and cells were seeded on the membrane and cultured in the medium McCoy's 5A (Gibco, USA). To avoid the direct interaction of liquid between the 6-well plate and an embedded chamber, a gasket plate was placed in-between.

2.5. *In vitro* anti-tumor efficacy

The human colon carcinoma HCT116 cells were purchased from the Cell Bank of the Chinese Academy of Sciences (CBCAS, China). The cells were cultured in McCoy's 5A culture medium supplemented with 10 vol % fetal bovine serum (FBS, Gibco, USA), 1 vol% penicillin & streptomycin (Gibco, USA). The human colonic epithelial cells (HCoEpiC) were obtained from Guangzhou Jennio Biotech Co., Ltd, and cultured in MEM culture medium (Corning, USA) with 10 vol% PBS and 1 vol% penicillin & streptomycin. All cells were passaged by digestion using 0.25 % trypsin (Gibco, USA) and incubated in an atmosphere of 5 % CO₂ at 37 °C. The incubator was set 5 % carbon dioxide and 20 % oxygen partial pressure.

The cell lines HCT116 and HCoEpiC were separately seeded in an H₂-emitting device and a real-time cell growth process was observed under a 3D cell explorer microscope (Nanolive, 3D Cell Explorer, Swiss). The viability of cells after exposed to hydrogen at different concentrations was tested by a Cell Counting Kit-8 assay (DOJINDO, Japan) at time points of t = 24, 48, and 72 h. Results were collected by a microplate reader (BioTek, ELX800, USA).

To detect the apoptosis of tumor cells induced by the released H₂, HCT116 cells were seeded in the H₂-emitting device. After 48 h incubation, cells were collected and stained with Fluorescein (FITC) Annexin V and Propidium Iodide (PI) solution (Sony Biotechnology, Japan). Then, cells were tested by a flow cytometer (Beckman Coulter, CytoFLEX S, USA) and analyzed by the software FlowJo (BD, USA).

The effect of H₂ on the distribution of the arrested cell cycle of HCT116 cells was tested by flow cytometry. Cells were prestained by PI/RNase staining buffer (BD, USA) and the distribution of the arrested cell cycle was analyzed by ModFit LT (Verity Software House, USA).

2.6. Detection of mitochondrial membrane potential and apoptotic cells

The tumor cells preseeded on the cell culture slide (\varnothing 24 mm) were flipped over and covered on the H₂-emitting device for 12 h. The Mitochondrial Membrane Potential and Apoptosis Kit (Beyotime, China) was added for 20 min. Cells were subsequently washed twice for 5 min with buffer and photographed by confocal laser scanning microscopy (CLSM, Leica, TCS SP8 STED 3X, Germany). Nuclei were stained by Hoechst.

2.7. Detection of cleaved caspase 3 and cytochrome C

After exposed to H₂ for 12 h, tumor cells were transferred and seeded in the cell culture slide. After fixation and washing, cells were blocked for 1 h, then stained with cleaved caspase-3 antibody or Cytochrome C Antibody (Abcam, UK) overnight at 4 °C on a shaker. The cells were counterstained with fluorescein isothiocyanate (FITC, ABCAM, USA) or allophycocyanin (APC, ABCAM, USA) conjugated secondary antibody for 1 h. Finally, the cells were washed with an Immunol staining wash buffer three times before observation by CLSM. Nuclei were stained with Hoechst.

2.8. RNA-sequencing and western blotting

To investigate the molecular mechanism of H₂-induced death of tumor cells, HCT116 cells were exposed to H₂ for 48 h before harvested. Cells without H₂ treatment were set as a control group. Total RNA was extracted using Trizol (Invitrogen, USA) according to manual instruction. Subsequently, total RNA was quantified using a NanoDrop and Agilent 2100 bio-analyzer (Thermo Fisher Scientific, USA). Oligo(dT)-attached magnetic beads were used to purify mRNA. The double-stranded PCR products were heated until denatured and circularized by the splint oligo sequence to get the final library. The single-strand circle DNA was formatted as the final library. To compare the differentially expressed genes (DEGs) between the H₂ and control group, the data were analyzed using bioinformatics tools, and only genes with a value of fold change ≥ 2 and a P-value < 0.05 were considered.

After 48 h H₂-treatment, tumor cells were collected and lysed. The protein content in the lysate was quantified by a BCA assay kit (Solarbio, China) to ensure an equal amount of protein. The protein was resolubilized in loading buffer, loaded onto 10 % SDS-polyacrylamide gels and then transferred to polyvinylidene fluoride membranes. The membranes were blocked in PBS with Tween 20 with 5% bovine serum albumin (BSA) and incubated with primary antibodies (diluted 1:1000; Cell Signaling Technology, USA) against p53, Cathepsins B, Bax, Bcl-2, and LC3B at 4 °C overnight. Then, the membrane was incubated with an HRP-linked antibody (diluted 1:2000; Cell Signaling Technology, USA) at 37 °C for 1 h. A ChemiDoc Imager system (Bio-Rad, ChemiDoc MP, USA) was used to measure the levels of specific proteins after the treatments.

2.9. Construction of solid tumor model

All animal experiments were approved by the Experiment Animal Ethics Committee of the Shanghai Jiao Tong University Affiliated Sixth People's Hospital. HCT116 cells (2×10^6) were suspended in PBS (50 μ L) and injected subcutaneously into the flank regions of 25 male BALB/c nude mice. After one week of inoculation, tumors grew up to a diameter of about 5 mm. These tumor-bearing mice were implanted with a titanium wire (\varnothing 1 \times 5 mm), or Mg wires (1 or 3 pieces, \varnothing 1 \times 5 mm). The mice without implanting any metallic wires were used as a blank control group. As a positive control, the mice were inhaled with 2 vol% H₂ persistently for 24 days. The size of tumors was recorded every four days and its volume (V) was calculated according to the formula: $V = ab^2/2$, where a (mm) and b (mm) represented the tumor length and width, respectively. The changes in body weight were recorded every

four days.

2.10. Analysis of histology and blood chemistry

On the 24th day, all mice from each group were sacrificed. Their tumor tissue and major organs were harvested to stain with hematoxylin and eosin (H&E) for histological evaluation. Tumors were stained by transferase-mediated deoxyuridine triphosphate nick end labeling (TUNEL) and caspase 3 for observation of their apoptosis. Meanwhile, the blood of mice in each group was harvested from the eye socket for microelement analysis and routine analysis of blood using an automatic analyzer (Hitachi, 7600-030, Japan).

2.11. TEM observation of tumor tissues

The tumor tissues were cut into about 1 mm³ piece and fixed with 2.5 % glutaraldehyde for 6 h at 4 °C. After a serial of standard procedures of dehydration and resin-embedding, the tissue samples were sliced by ultramicrotome system (Leica, EM UC7FC7, Germany) for about 60 nm in thickness, stained with both uranyl acetate and lead citrate for 15 min before imaged using TEM (Thermo Fisher Scientific, Talos L120C G2, USA).

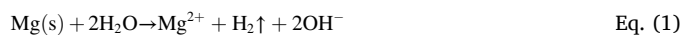
2.12. Statistical analysis

All data were expressed as mean \pm SD, and statistical analysis was performed using Student's t-test. Statistical significance is denoted by * $p < 0.05$, ** $p < 0.01$ and *** $p < 0.001$.

3. Results

3.1. Controlled release of H₂ by varying medium pH and exposed surface area of Mg

In an aqueous environment, Mg dissolves to form Mg²⁺ ions (the anodic reaction) and hydrogen (the cathodic reaction) as shown in Eq. (1).



As shown in Fig. 1, by changing the exposed surface area of the material and the medium pH values, a variable and controlled released of hydrogen from Mg could be achieved. When the exposed surface area of Mg to the PBS solution increases from 12 mm²/mL to 48 mm²/mL, the total volume of released hydrogen increased by 258.70 \pm 36.31 % in the first 12 h. Accordingly, the concentration of hydrogen dissolved in PBS also elevates from 98.50 \pm 6.76 μ M to 236.50 \pm 10.50 μ M. To study the effect of pH on the release rate of hydrogen, the pH values of PBS (i.e., 5.6, 6.5, and 7.4) were adjusted by adding HEPES powders. Decreasing the medium pH values from 7.4 to 5.6 accelerated the propensity of corrosion, evidenced by the elevated open circuit potential from -1.57 ± 0.11 mV to -1.91 ± 0.13 mV (Fig. S1). The corrosion current densities (I_{corr}) of Mg in PBS with pH = 6.5 was $(3.27 \pm 0.39) \times 10^{-4}$ mA cm⁻² V.S $(6.10 \pm 0.19) \times 10^{-5}$ mA cm⁻² in neutral solution (pH = 7.4) (Supplementary Table 1). Due to the faster corrosion of Mg at a lower pH medium (pH = 5.6), the released hydrogen was 147.40 times higher than that in neutral PBS, and the dissolved hydrogen in the near steady-state also increases by 0.93 folds. The pH-responsive release rate of hydrogen was also confirmed in the cell culture solution under 5% CO₂ atmosphere (see Fig. S2). As the pH value of the immersion solution decreased, the near-equilibrium concentration of dissolved H₂ in the culture medium was 44.50 \pm 2.18 μ M (pH = 7.4), 61.83 \pm 2.75 μ M (pH = 6.5), and 82.33 \pm 3.21 μ M (pH = 5.6). These observations suggest that the concentration of dissolved hydrogen in simulated physiological solutions can be regulated by controlling the corrosion rate of Mg, either by changing the specific surface area

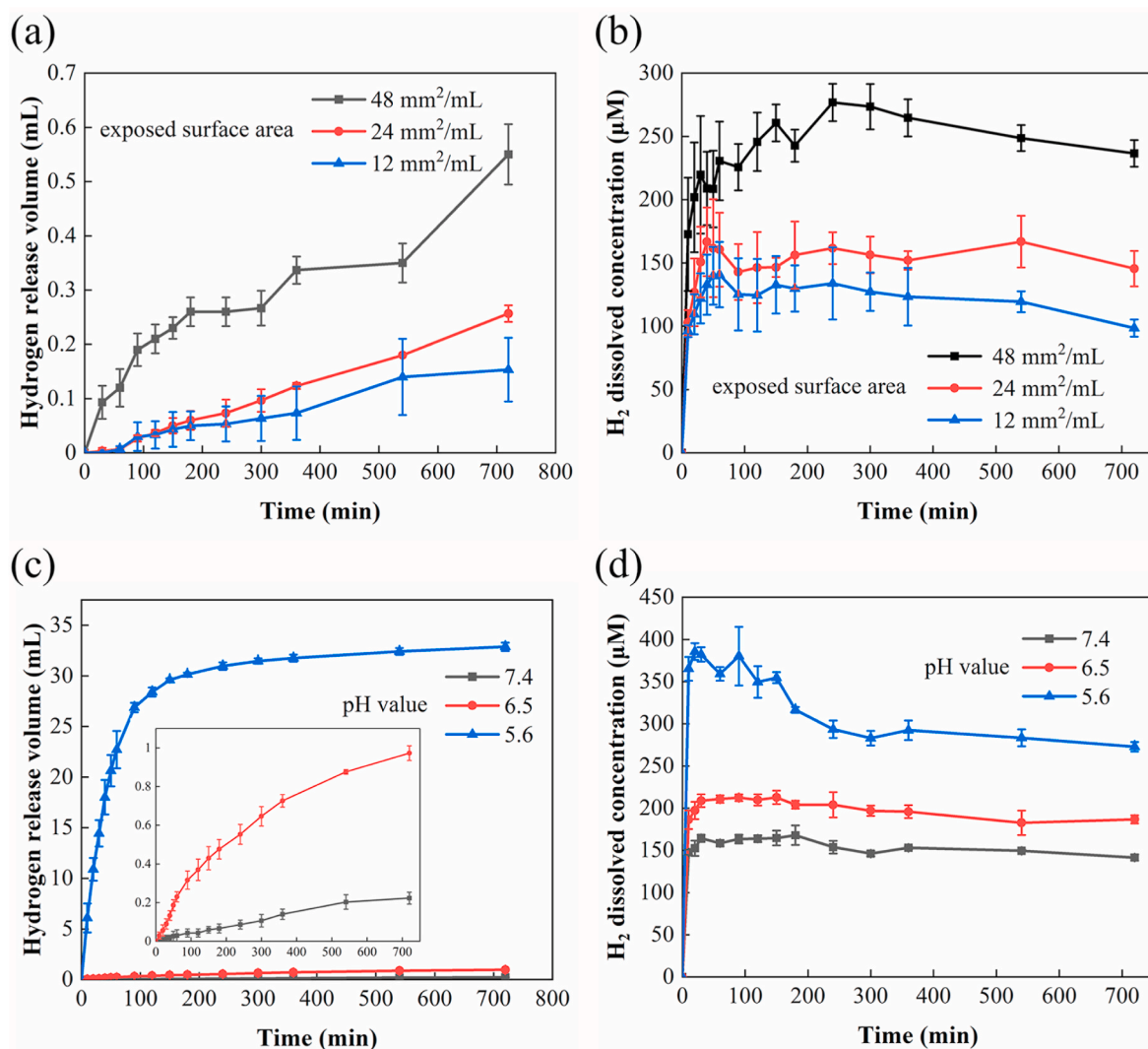


Fig. 1. Controlled release kinetics of hydrogen achieved by changing the surface area of Mg or the pH value of PBS. (a) The volume of released H₂ and (b) the concentration of dissolved H₂ in PBS solution increased with the exposed surface area (mm² per mL PBS) of Mg plates (pH = 7.4). (c) The volume of released H₂ and (d) the concentration of dissolved H₂ in PBS increased as the pH value decreases.

exposed to the surrounding medium or adjusting the medium pH values.

3.2. The anti-tumor efficacy of H₂ *in vitro*

In order to study the effect of H₂ released alone on human colon carcinoma HCT116 cells, a special *in vitro* set-up using a transwell system was employed. As presented above, the controlled and variable release of H₂ from Mg was achieved by varying the pH of PBS. Sample and extraction vehicles were placed on the well and the cells in the upper chamber.

We first monitored the morphology of HCT116 cells by immersing cells in an H₂-containing culture medium and observed them under a live-cell imaging microscope. HCT116 cells exposed to the H₂-rich medium underwent apoptosis after 2 h of incubation. As shown in Fig. 2a and Movie 1, tumor cells exhibited a spindle-shaped morphology at the beginning, but then shrank into an oval shape after 2 h. As time proceeds, cell division was halted and a secreted apoptotic body was expelled extracellularly, as denoted by the red box in Fig. 2a. In comparison, tumor cells without hydrogen treatment remained intact. Furthermore, hydrogen exposure did not harm normal tissue cells or change their morphology, as shown by imaging the human colonic epithelial cells HCoEpiC under the same conditions (Movie 2 and

Fig. S3).

Supplementary video related to this article can be found at <https://doi.org/10.1016/j.bioactmat.2021.07.026>.

To quantitatively assess the effect of hydrogen exposure on proliferation, apoptosis, and division of cells, we cultured normal tissue cells and tumor cells in a culture medium with different concentrations of dissolved hydrogen and measured the corresponding cell viability after 24–72 h. As representatives, cell culture medium with a relatively low H₂ concentration of $44.50 \pm 2.18 \mu\text{M}$ H₂ (defined as L-H₂ group) rarely affected the proliferation of tumor cells in the first 48 h, as observed in treatment without hydrogen (Fig. 2c). After 72 h, the proliferation rate in the L-H₂ group was reduced by less than 14.54%. When the concentration of dissolved hydrogen was increased to $61.83 \pm 2.75 \mu\text{M}$ (defined as M-H₂ group), compared with the treatment without H₂, the number of tumor cells declined by $90.47 \pm 1.62\%$ after 72 h. Monitoring of the cell cycle progression suggested these tumor cells were arrested in the G₀/G₁ phase (Fig. 2d). The ratio of apoptotic cells was also measured by flow cytometry (Fig. 2e). The results showed that the apoptotic level of HCT116 cells in the M-H₂ treatment was $35.96 \pm 0.73\%$, a much higher apoptotic rate than that in the L-H₂ group ($10.56 \pm 1.21\%$). While a relatively high level of dissolved hydrogen inhibited the proliferation of tumor cells (Fig. 2c), the proliferation of normal tissue cells

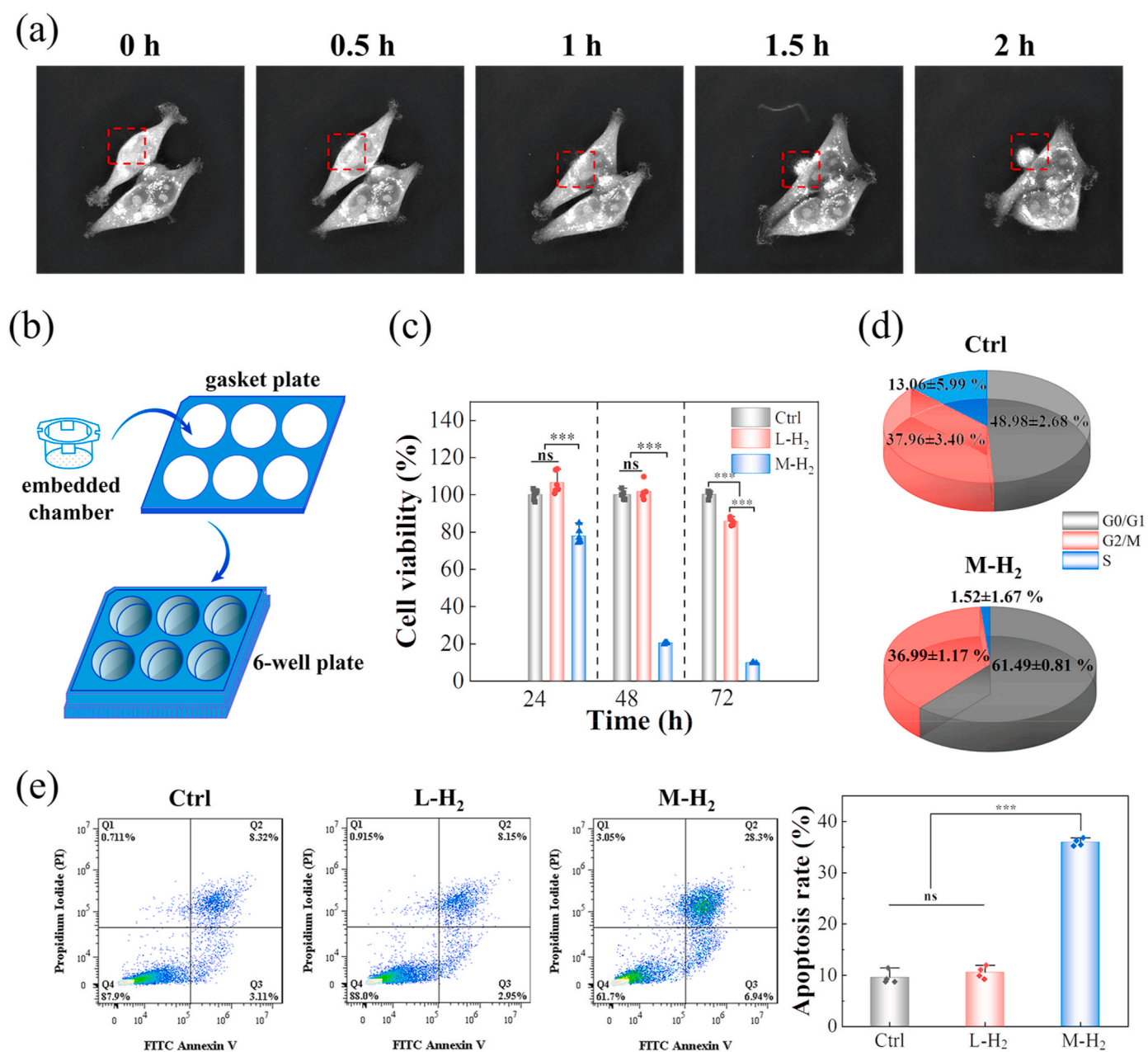


Fig. 2. Hydrogen induces tumor cell apoptosis at certain critical concentrations. (a) A series of morphology images of HCT116 cells from a live cell imaging microscope. (b) Schematic illustration of H₂-emitting device. (c) The cell viability of HCT116 cells with different treatments. (d) The cell cycle of the HCT116 cells in the Ctrl and M – H₂ groups; and (e) flow cytometry of cell apoptosis after different treatments and the corresponding apoptosis rate was statistically quantified. L-H₂ and M – H₂ groups represent the low and medium concentrations of H₂ in the culture medium, respectively. The ctrl group represents no H₂-treatment.

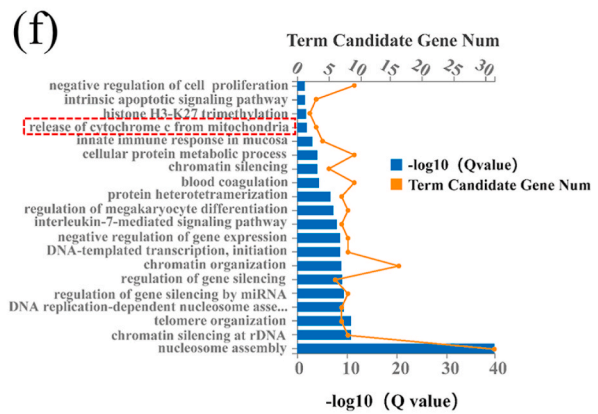
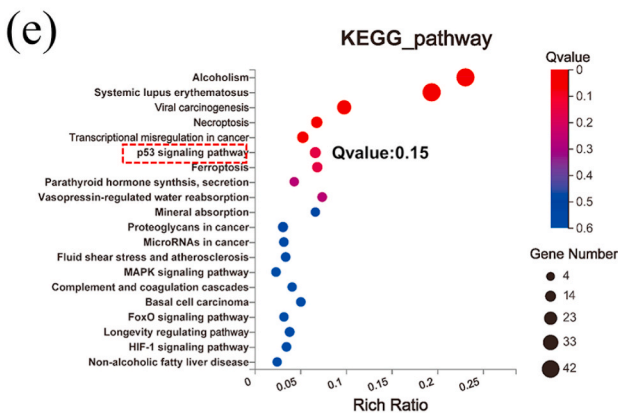
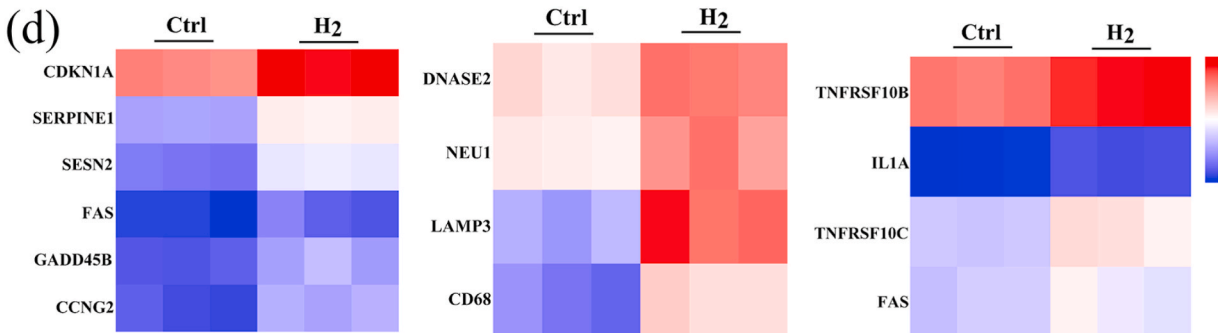
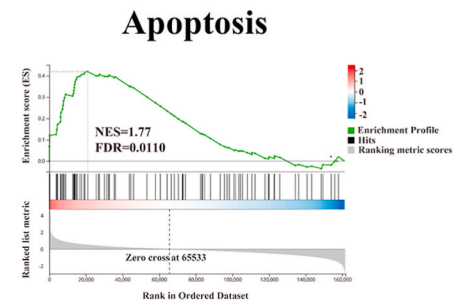
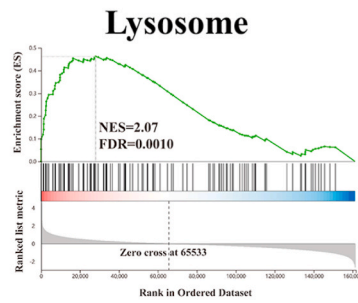
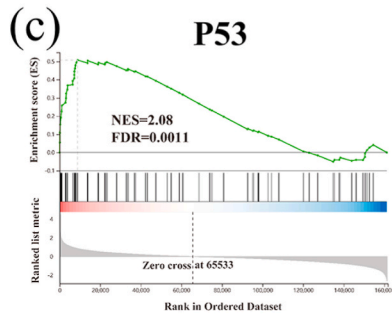
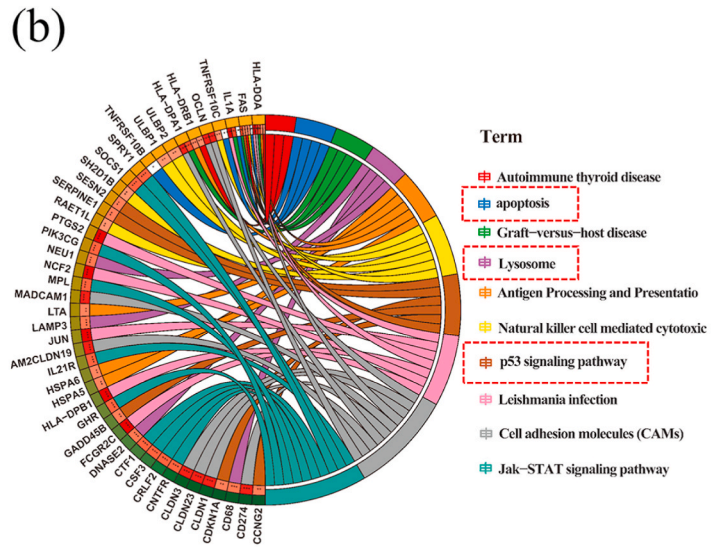
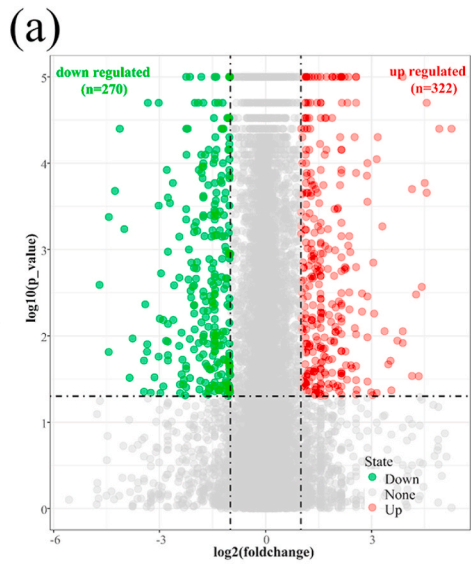
HCoEpiC was not affected after being exposed to a high dose of hydrogen for 72 h (Fig. S4).

Previous studies have attributed the anti-tumor efficacy of hydrogen to cytotoxic ROS decrease in tumor cells. To more accurately measure the effect of H₂ on ROS, we performed a semi-quantitative analysis of ROS by flow cytometry. Meanwhile, the marker of oxidative stress malondialdehyde (MDA) and the antioxidant enzyme superoxide dismutase (SOD) were quantified analysis by a plate reader (Figs. S5 and S6). Compared to the control group without H₂ exposure, both semi-quantitative and quantitative measurements confirmed a significant reduction ($p < 0.05$) in the ROS level after the M – H₂ treatment. However, no statistical difference in ROS level was observed among the L-H₂ and M – H₂ groups. Since the M – H₂ group exhibited much stronger anti-tumor activity than the L-H₂ group (see Fig. 2) but no difference in ROS level was observed, we assumed that other

mechanisms than the intracellular ROS decrease were involved in the anti-tumor activity of H₂.

3.3. Identification of the apoptosis signaling pathway activated by H₂

To explore the potential anti-tumor mechanism of H₂, we conducted mRNA transcriptome analysis. About 600 differently expressed genes (DEGs) were identified in the H₂-treated group relative to the Ctrl group (no H₂-treatment), including 322 up-regulated genes and 270 down-regulated genes ($P < 0.05$, fold change > 2 ; Fig. 3a). According to the molecular signatures database (MSigDB) [31], a gene set enrichment analysis (GSEA) was conducted. Results are shown in Fig. 3b and c (abbreviations and full names of the genes can be found in Table S2). We found that DEGs were mainly enriched in pathways associated with P53 signaling (*CDKN1A*, *SERPINE1*, *SESN2*, *FAS*, *GADD45B* and *CCNG2*),



(caption on next page)

Fig. 3. Hydrogen regulated gene expressions related to the P53-mediated apoptosis signaling pathway. (a) A volcano plot showing up/down-regulated genes after M – H₂ treatment vs. the Ctrl group. Genes with an absolute fold change of >2 and a P value of <0.05 are highlighted in green and red color separately, denoting the down- and up-regulated genes, respectively. (b) Circular visualization of the gene-annotation enrichment analysis after gene set enrichment analysis (GSEA) was conducted using the Molecular Signatures Database (MSigDB). (c) The gene set enrichment analysis of the P53, lysosome and apoptosis pathway. (NES: normalized enrichment score). (d) A heat map of differentially expressed genes associated with three apoptotic pathways after H₂ treatment, a fold change of >2 and a P value of <0.05 compared to the Ctrl group was analyzed. (e, f) An analysis of the enriched differentially expressed genes using the Kyoto Encyclopedia of Genes (KEGG) and Genomes (GO) database.

lysosome signaling (*DNASE2*, *NEU1*, *LAMP3*, and *CD68*), and apoptosis signaling (*TNFRSF10B*, *IL1A*, *TNFRSF10C*, and *FAS*) (Fig. 3d). The DEGs enrichment analyses were also carried out using multiple databases including the Kyoto Encyclo-pedia of Genes and Genomes (KEGG) [32] and the Gene Ontology (GO) databases [33]. In H₂-treated cells, KEGG and GO databases suggested an enhanced expression of genes associated with the P53 signaling pathway (highlighted by a red box in Fig. 3e) and with the release of cytochrome C from mitochondria (Fig. 3f, highlight by a red box), respectively. According to these results, we speculated that H₂ could induce the apoptosis of tumor cells by up-regulating the P53-mediated lysosome/mitochondria pathway.

In order to prove the P53 regulated anti-tumor mechanism of H₂, we next tested the expressions of selected proteins via western blotting and immunofluorescence. As shown in Fig. 4a, the immunoblotting analyses revealed that H₂ up-regulated the expression of the P53, cathepsin B,

and Bax/Bcl-2. The up-regulation of P53 can initiate the lysosomal leakage to release cathepsin B, which further activated Bax/Bcl-2 to permeabilize the outer membrane of mitochondria [34,35]. This permeabilization results in the depolarization of the mitochondrial membrane and a decrease in the mitochondrial membrane potential (MMP), as demonstrated by the mitochondrial membrane staining with Mito-Tracker Red CMXRos in Fig. 4b. Due to the mitochondrial outer membrane damage, adenosine triphosphate (ATP) from the inner mitochondrial membrane and pro-apoptotic protein cytochrome c were released (Fig. 4c and Fig. S7). Since the release of cytochrome c often leads to the activation of downstream caspase-3, the expression of caspase-3 was evaluated by using a cleaved caspase-3 antibody. As shown in Fig. 4d and Fig. S8, the expression of cleaved caspase-3 increased significantly in the H₂-treated group, which is a typical hallmark of cell apoptosis [36]. Furthermore, the confocal microscopy

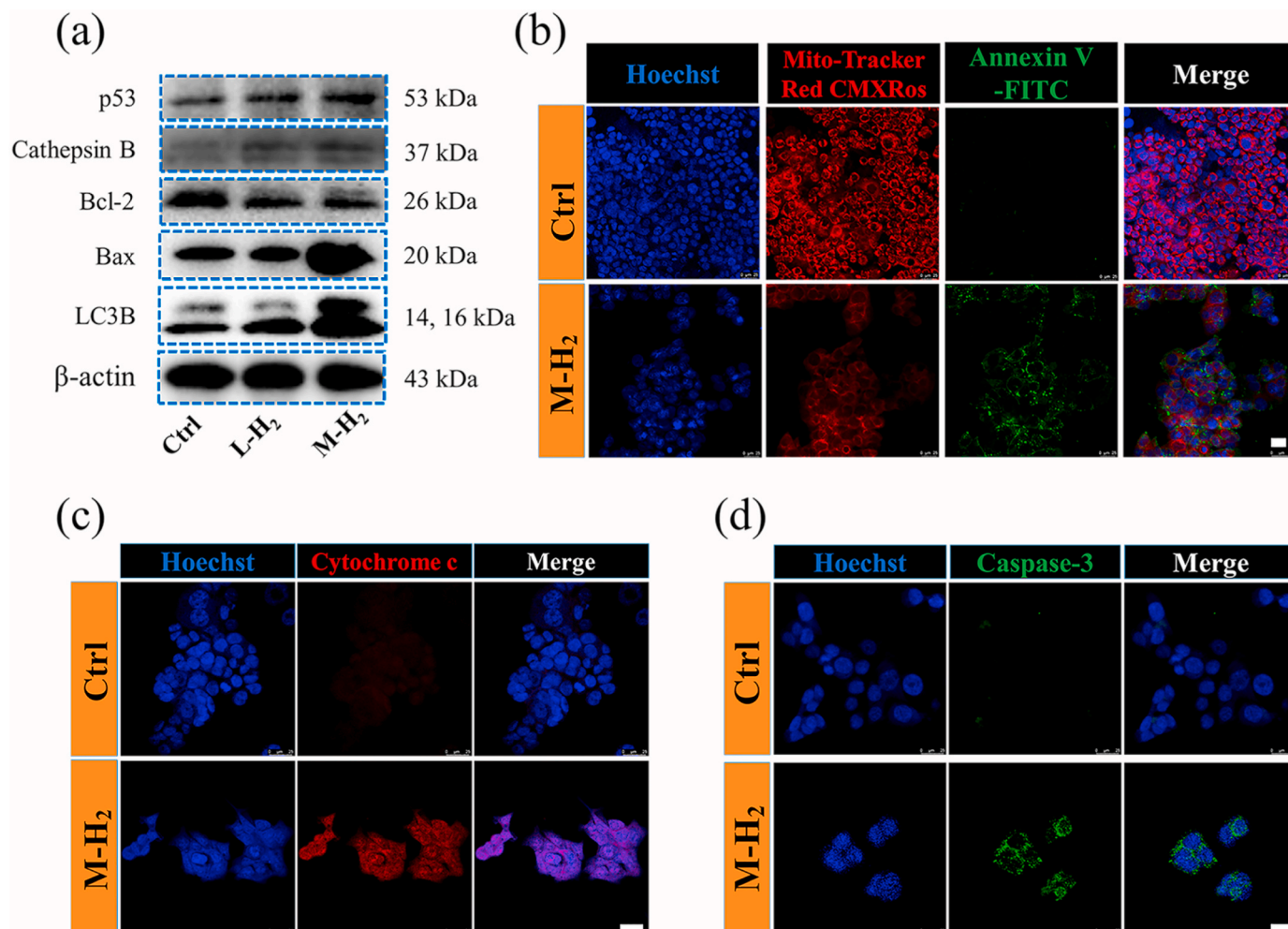


Fig. 4. The up-regulated P53 activates the mitochondrial apoptosis pathway by hydrogen. (a) The P53, cathepsins, Bax, Bcl-2 and LC3B expression after M – H₂, L-H₂ and Ctrl treatment, respectively. (b) Confocal fluorescence images of mitochondria membrane potential and apoptosis of HCT116 with or without H₂ treatment. The mitochondria membrane potential was stained by Mito-Tracker Red CMXRos (red), apoptosis cells were stained by Annexin V-FITC (green) and the nuclei were stained by Hoechst 33342 (blue). The scale bar is 25 μ m. (c) The analysis of cytochrome C expression in HCT116 cells using the APC-conjugated cytochrome C antibody. Scale bar: 25 μ m. (d) The analysis of the caspase-3 expression in HCT116 cells using FITC-conjugated cleaved caspase-3 antibody. Scale bar: 25 μ m.

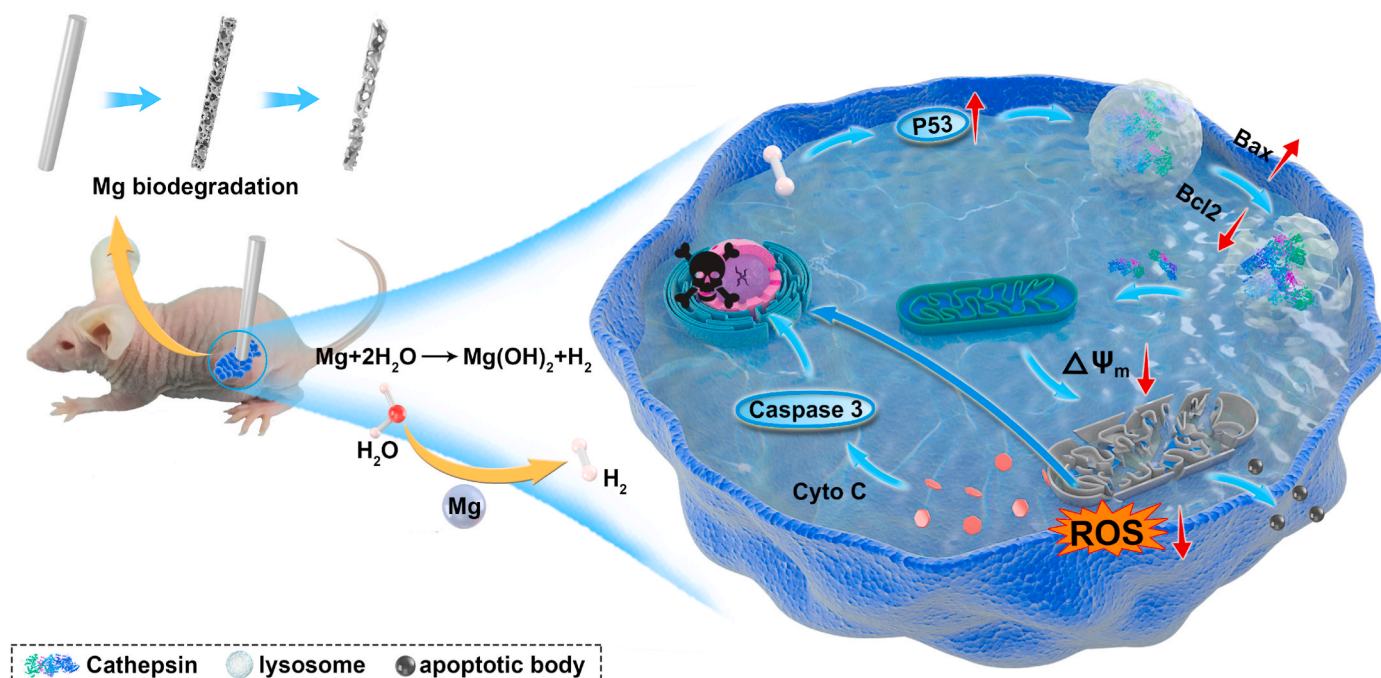
images exhibited that mitochondria (green) and lysosome (red) were colocalized (yellow) after H₂ treatment (Fig. S9), indicating that damaged mitochondrion was degraded by lysosomes leading to apoptotic bodies generation. In addition, the microtubule-associated protein 1 light chain-3B (LC3B) is an autophagy protein, which mediates the progression of apoptosis [37]. We found that the release of H₂ increases the expression LC3B protein, consistent with the phenomenon observed in Movie 1. In summary, with RNA sequencing and relative protein expression analyses, we found the H₂-mediated apoptosis of tumor cells was induced by the up-regulation of P53 through a lysosome-mitochondrial pathway, as depicted in Scheme 1.

3.4. The anti-tumor efficacy of H₂ in vivo

The anti-tumor performance of H₂ after implantation of Mg was further investigated *in vivo*. Balb/c nude mice injected with HCT116 cells in the right flank were used to establish a model of tumor xenografts and randomly divided into five groups, including a control (Ctrl) group, one titanium wire implanted (Ti) group, one Mg wire implanted (Mg1) group, three Mg wires implanted (Mg3) group and an H₂ inhalation (H₂) group. By comparing with the Ti material, a clinical rectal anastomotic staple without anti-tumor property, we study the inhibitory effect of H₂ on tumors *in vivo* by changing the exposed surface area of Mg wire. Considering the complicated environment in the body, an H₂-inhalation group (2 vol% H₂-98 vol% O₂ mixture) was set to individually study the anti-tumor efficacy of H₂ on tumors, which excludes the effect of two other degradation products of Mg on tumors *in vivo*. As shown in Fig. 5a, Mg wires were inserted into the tumor tissue to generate H₂ *in situ*. After 8d, 16d, and 24d implantation, the degradation behavior, as well as volume loss of Mg wires in tumor tissue, was assessed by micro-computed tomography (micro-CT; Fig. 5b). The release rate of hydrogen could be estimated from the volume change of Mg implants. Since no apparent hydrogen bubble was observed around the tumor, we assumed the average concentration of hydrogen dissolved in body tissue did not reach a saturated state, so the average H₂ concentration should be proportional to the release rate of hydrogen (μL/d) from Mg implants (Fig. S10). The average hydrogen release rate can be estimated from the average corrosion rate of Mg based on micro-CT imaging. We defined a

nominal hydrogen concentration, $\rho_{H_2} = R_{H_2}/V_{T0}$, where R_{H_2} is the hydrogen release rate (μL/d), and V_{T0} is the volume of tumors at time zero. The local concentration of hydrogen, C_{H_2} , is proportional to the normal H₂ concentration through $C_{H_2} = \eta \cdot \rho_{H_2}$, where η is the volumetric ratio of hydrogen dissolved in tumors to the total hydrogen produced by Mg. η is roughly estimated on the order of ~14 % from the *in vitro* immersion test. After implantation for 24 days, about 1/3 of Mg wire was degraded and the hydrogen release rate of Mg was constantly maintained at about 80.05 μL/d (Fig. 5c). When the exposed surface area of Mg was increased from 17.3 mm² to 51.9 mm², the estimated local concentration of hydrogen from 91.2 μL/d/mm³ to 273.6 μL/d/mm³; accordingly, the volume of tumors at 24 d declined by 64%. In contrast, both the blank Ctrl group without implants and Ti wire-implanted mice exhibited a rapid progression of the tumor. The tumor-bearing mice treated by H₂, either administrated through direct inhalation H₂ or transplanted with Mg wires exhibited significantly suppressed tumor growth and weight (Fig. 5d and e). Impressively, tumor tissue necrosis occurred around the Mg wires, while the tumor tissue around the Ti wires grew well (Fig. S11). During the process of therapy, no obvious body weight loss in all five groups of mice was observed (Fig. 5f). Meanwhile, analysis of alanine aminotransferase (ALT), aspartate aminotransferase (AST), creatinine (CRE), lactate dehydrogenase (LDH), and creatine kinase MB (CK-MB) by blood chemistry showed no distinct abnormality in Mg-implanted groups. Furthermore, no obvious pathological changes were found in the normal tissues after the different treatments (Fig. S12), highlighting the biocompatibility of Mg-implanted H₂ therapy *in vivo*.

In addition, the ultrastructure of tumor tissue and cells was investigated by transmission electron microscopy (TEM). As a comparison, the tumor cells in the Ctrl and Ti group demonstrated clear cell boundaries in an oval shape and evenly distributed chromatin in the cell nucleus. In the Mg-implanted group, upon the administration of H₂, chromatin aggregated and touched the nuclear membrane and cell boundary became blurry, revealing early signs of apoptosis. Furthermore, a necrotic tissue wrap was found around the Mg wires. A TEM image of this necrotic tissue revealed that the nucleus membrane of tumor cells broke up and the cell nucleolus turned into smooth intranuclear masses. As mitochondria were engulfed by the lysosome, some vacuolated



Scheme 1. Schematic illustration of the anti-tumor effect of H₂ from biodegradable Mg.

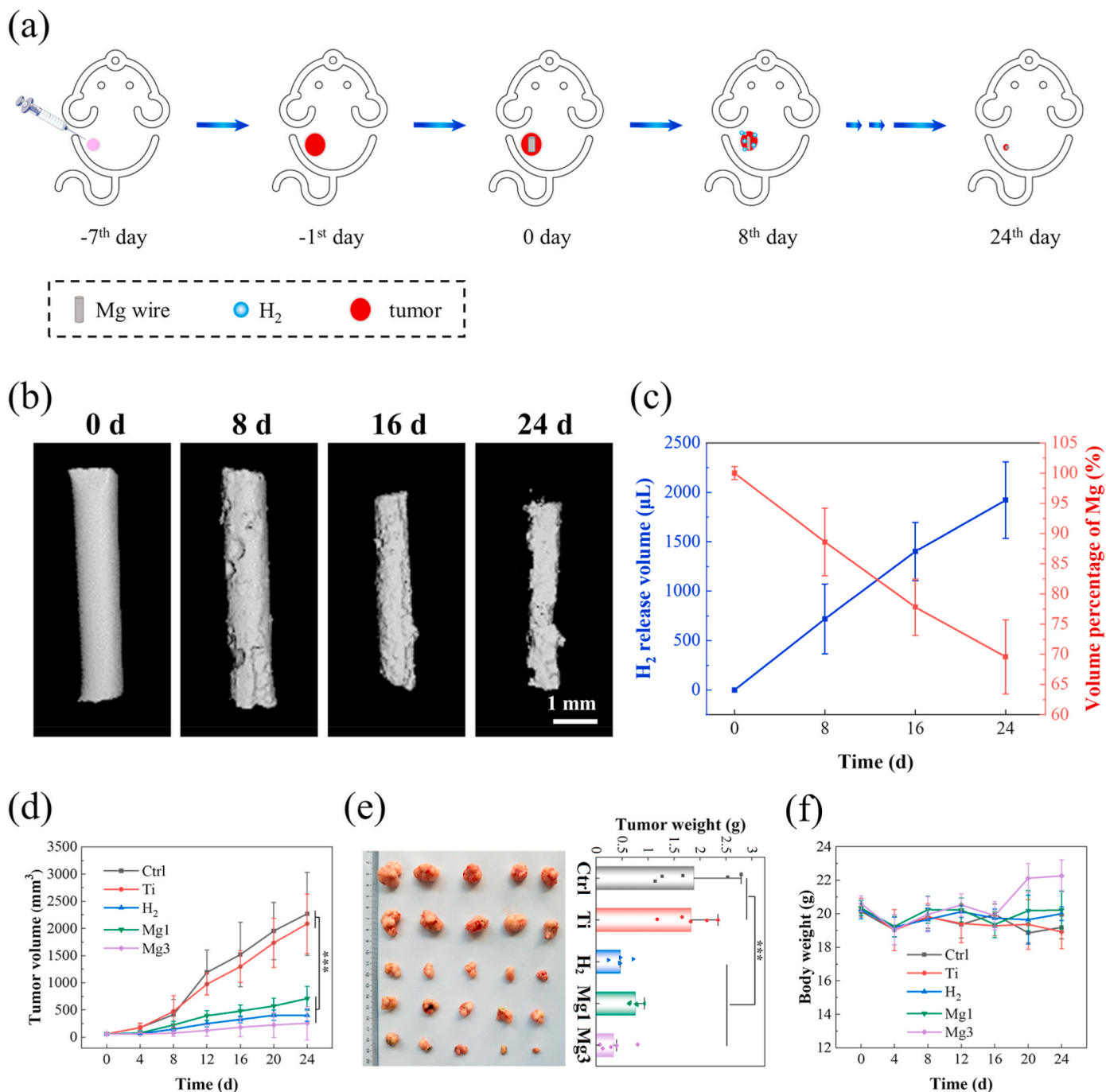


Fig. 5. Hydrogen released from Mg wires inhibits tumor growth *in vivo*. (a) The anti-tumor evaluation of the H₂ therapies through Mg degradation on tumor-bearing mice. (b) Micro-CT images of Mg wires after 0 d, 8 d, 16 d, and 24 d implantation in tumor tissue; (c) Evolution of hydrogen released and wire volumes in tumor-bearing mice after 8 d, 16 d and 24 d implantation. (d) Growth curve of tumor volume after different treatments. (e) The HCT116 tumor weight and the corresponding representative pictures of tumors at the end of the experiment. (f) Bodyweight change after different treatments.

mesostructures were observed, and apoptotic bodies were formed (Fig. 6a and Fig. S13a). Immune cells including foreign body multinucleated giant cells and neutrophils were recruited (Fig. S13b). In the distal end of Mg wires, tumor cells underwent an early stage of apoptosis (Fig. S14). Histological examination and immunofluorescence stainings showed that the tumor cells in the Mg-implanted group exhibited most cell shrinkage and loss of nuclei, indicating apoptosis (Fig. 6b). Inhalation of H₂ resulted in less intensive apoptosis, compared to a negligible extent of apoptosis in the blank Ctrl or Ti-implanted group. The therapeutic effectiveness, *i.e.*, anti-tumor activity through induction of apoptosis of Mg implantation was assessed by deoxyribonucleic acid

(DNA) fragmentation *via* terminal deoxynucleotidyl transferase (TdT)-mediated dUTP nick end labeling (TUNEL) assay (Fig. 6c) and caspase 3 stainings (Fig. 6d). A maximum number of apoptotic cells (green) was detected in the Mg-implanted group. Quantification showed that the apoptosis rate in the Mg-implanted group was 14.46-fold higher than in the blank Ctrl group (Fig. S15). Compared to the other groups, immunofluorescence staining results showed that caspase 3 (green fluorescence) was up-regulated in the Mg-implanted group (Fig. 6d). In summary, Mg implantation exhibited excellent *in situ* anti-tumor therapeutic outcomes *in vivo*, and the anti-tumor efficacy could be controlled by adjusting the exposed surface area of Mg implants.

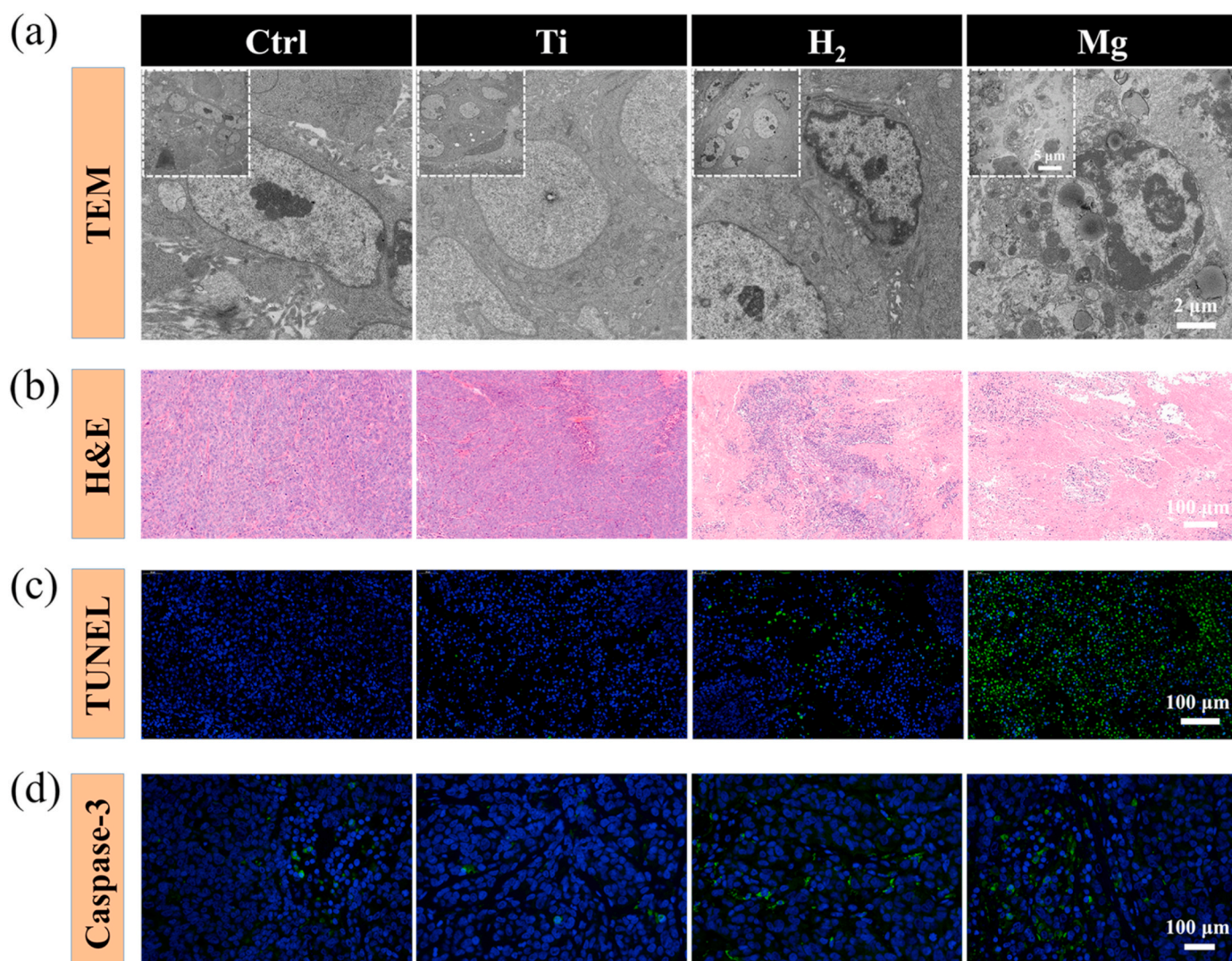


Fig. 6. Hydrogen induces tumor tissue apoptosis in tumor-bearing mice. (a) TEM photos of the tumor tissues at various scales; (b) H&E images of tumor tissues dissected from each group after different treatments on day 24; (c) Apoptosis was analyzed by TUNEL staining in tumor tissue after 24 days of treatment; (d) Confocal laser scanning microscopy of caspase-3 staining in tumor tissues after different treatments.

4. Discussion

H₂ gas is considered to be a therapeutic medical agent, which exhibits remarkable effects in some diseases, especially in tumors. Currently, some methods of H₂-treatment trials are being attempted, including inhalation of H₂ gas [14], drinking H₂-enrich water [16], and nanomaterials releasing [38]. However, due to the low efficacy of external delivery and potential metabolic toxicity of nanomaterials, H₂-administration remains a huge challenge.

In the present study, we were able to control the release of H₂ from biodegradable magnesium-based biomaterial, which inherent degradation releases H₂, allowing a localized hydrogen delivery stimulated by the acidic tumor microenvironment. Evidence from the *in vitro* and *in vivo* findings suggested that H₂ induced tumor cells apoptosis when the dissolved H₂ exceeds a certain concentration. Apart from the well-accepted mechanism that the H₂ selectively decreases ROS [5], we found another underlying mechanism of H₂ for the anti-tumor effect. To a large extent, the molecular H₂ increased the expression of tumor suppressor protein P53 and subsequently activated the mitochondria-related apoptosis pathway.

Although it has long been known that the P53 served as a target to mitochondria for tumor therapy [39,40], the exact role of P53 in

medical H₂ treatment for anti-tumor is unclear. Several points of our findings support that hydrogen can induce tumor cell apoptosis with the involvement of P53, which acts as an important role in tumor progression as well as apoptosis [41]. We recorded the dynamic behavior of human colon carcinoma cells in real-time and found an apoptotic body released from cells after treatment with H₂ from Mg degradation (Fig. 2a & Movie 1). Compared to the cells without H₂ treatment, the analysis of paired comparative bioinformatics through different databases suggested that the apoptotic cells were mainly attributed to the up-expression of P53, which interrupt the activities of tumor cells, such as DNA repair, metabolism and antioxidant response [42]. Furthermore, the underlying mechanism was further proved by the western blotting and immunofluorescent staining method. The up-regulated P53 activated the signaling to broke the mitochondrial membrane and release the pro-apoptotic protein. The damaged mitochondria were dissolved by lysosomes to form apoptotic bodies and then were released outside the cell.

Compared to the clinical usage of Ti material, the H₂ carrier of Mg material showed unexpected anti-tumor efficacy *in vivo*. In our findings, Mg implants inhibited the growth of tumor tissues by continuously releasing H₂ *in situ* for 24-day observation. The volume of tumors in the control group is about 9 times than that in the Mg3 group after 24d

treatment. Furthermore, a large number of apoptosis cells and necrotic tissue were found surrounding the Mg wires (Fig. 6 and Fig. S11). By increasing the exposed surface of Mg wire, more H₂ concentration in solid tumors induces more cell apoptosis and a slower growth rate of tumors. These findings are consistent with the result *in vitro*. Nevertheless, whether the two other degradation products of Mg affect tumor cells was hard to identify. Therefore, tumor-bearing mice were put into a box saturated with 2 % H₂ and individually studied the effect of the molecular H₂ on the growth of tumors. The outcome suggested that the H₂ is a promising trial for tumor-inhibiting. The employment of Mg implants for the *in vivo* delivery of H₂ has several advantages over traditional H₂-inhalation therapy. 1) The tumor microenvironment (TME) accelerates the release of hydrogen from Mg. TME is characterized by declined pH value, which accelerates the degradation of Mg wire. This triggers a pH-responsive release of H₂ from Mg wire (Fig. 1), which increases the local concentration of hydrogen and improves its antitumor efficacy (Fig. S4). The release of hydrogen by Mg implantation achieves a localized delivery around the tumor, can increase the concentration of hydrogen around the implantation site, thus improving the anti-cancer effect. 2) Portability. The Mg implants with a low density are easy to carry on, which does not require a heavy tank for direct H₂ inhalation. 3) High H₂-generation capacity. A small volume of 1 cm³ pure Mg implants can generate as much as 1600 mL hydrogen around tumors. In a hypothetical calculation, three Mg wires with a dimension of $\Phi 1 \times 5$ mm can generate 5.74 mL H₂ within 24 days, which is as effective as inhaling 30 L H₂-O₂ mixture gas for suppression of tumor, as shown in Fig. 5d. Hence, it is reasonable to believe that the degradable Mg implants showed more therapy efficiency in H₂-delivery to tumor tissue than H₂-inhalation. More importantly, our results indicate that the activation of tumor cell apoptosis requires a minimum inhibitory concentration of hydrogen around 91.2 $\mu\text{L}/\text{d}/\text{mm}^3$, which provides reference standards of dosage for the application of medical hydrogen in the field of oncology. In our previous work, Mg ions were regarded as an indispensable role to inhibit bone tumor cell growth [29]. Therefore, whether H₂ and Mg ions have a synergistic effect *in vitro* and *in vivo* awaits further investigation. It would also be important to test whether H₂ could affect other types of tumor cells.

5. Conclusion

In conclusion, we showed an H₂ concentration-dependent suppression of tumor cells HCT116 induced by the degradation of Mg. The concentration of hydrogen dissolved in body fluid can be regulated by controlling the degradation rate of Mg, such as varying the medium pH value or the specific surface area exposed to the immersion solution. Because of the emission of H₂ from Mg, the expression of tumor suppressor protein P53 was up-regulated to induce tumor cells apoptosis through a lysosome-mitochondria-mediated apoptosis signaling pathway. Mg wires inserted in tumor-bearing mice also confirmed its anti-tumor therapy efficacy by releasing hydrogen gas *in situ*. These results indicated that the controlled release of hydrogen from Mg implants (or anastomotic staple) has great potential for the suppression of colorectal cancer.

CRedit authorship contribution statement

Rui Zan: and designed the study. **Hao Wang:** and performed the experiments. **Weijie Cai:** performed the experiments. **Jiahua Ni:** and wrote the manuscript. **Bérenère J.C. Luthringer-Feyerabend:** wrote the manuscript. **Wenhui Wang:** prepared the Mg material. **Hongzhou Peng:** and prepared the Mg material. **Weiping Ji:** assisted in the animal experiment and provided some advises. **Jun Yan:** and assisted in the animal experiment and provided some advises. **Jiazeng Xia:** assisted in the animal experiment and provided some advises. **Yang Song:** designed the study. **Xiaonong Zhang:** designed the study.

Declaration of competing interest

The authors declare no competing interests.

Acknowledgments

The authors are grateful for support from the National Key Research and Development Program of China (No.2018YFC1106600) and the Interdisciplinary Program of Shanghai Jiao Tong University (No. ZH2018QNB07). Thanks to Xinyue Liu (Massachusetts Institute of Technology, MIT) for suggestions for this paper.

Appendix A. Supplementary data

Supplementary data to this article can be found online at <https://doi.org/10.1016/j.bioactmat.2021.07.026>.

References

- [1] W.-L. Wan, Y.-J. Lin, H.-L. Chen, C.-C. Huang, P.-C. Shih, Y.-R. Bow, W.-T. Chia, H.-W. Sung, In situ nanoreactor for photosynthesizing H₂ gas to mitigate oxidative stress in tissue inflammation, *J. Am. Chem. Soc.* 139 (37) (2017) 12923–12926.
- [2] Y. Wu, M. Yuan, J. Song, X. Chen, H. Yang, Hydrogen gas from inflammation treatment to cancer therapy, *ACS Nano* 13 (8) (2019) 8505–8511.
- [3] K. Imai, T. Kotani, H. Tsuda, Y. Mano, T. Nakano, T. Ushida, H. Li, R. Miki, S. Sumigama, A. Iwase, A. Hirakawa, K. Ohno, S. Toyokuni, H. Takeuchi, T. Mizuno, A. Suzumura, F. Kikkawa, Neuroprotective potential of molecular hydrogen against perinatal brain injury via suppression of activated microglia, *Free Radical Bio. Med.* 91 (2016) 154–163.
- [4] L. Zhang, P. Zhao, C. Yue, Z. Jin, Q. Liu, X. Du, Q. He, Sustained release of bioactive hydrogen by Pd hydride nanoparticles overcomes Alzheimer's disease, *Biomaterials* 197 (2019) 393–404.
- [5] I. Ohsawa, M. Ishikawa, K. Takahashi, M. Watanabe, K. Nishimaki, K. Yamagata, K. Katsura, Y. Katayama, S. Asoh, S. Ohta, Hydrogen acts as a therapeutic antioxidant by selectively reducing cytotoxic oxygen radicals, *Nat. Med.* 13 (6) (2007) 688–694.
- [6] M. Dole, F.R. Wilson, W.P. Fife, Hyperbaric hydrogen therapy: a possible treatment for cancer, *Science* 190 (1975) 152–154.
- [7] F.Y. Li, S.X. Zhu, Z.P. Wang, H. Wang, Y. Zhao, G.P. Chen, Consumption of hydrogen-rich water protects against ferric nitrilotriacetate-induced nephrotoxicity and early tumor promotional events in rats, *Food Chem. Toxicol.* 61 (2013) 248–254.
- [8] D. Wang, L. Wang, Y. Zhang, Y. Zhao, G. Chen, Hydrogen gas inhibits lung cancer progression through targeting SMC3, *Biomed. Pharmacother.* 104 (2018) 788–797.
- [9] J. Runtuwene, H. Amitani, M. Amitani, A. Asakawa, K.C. Cheng, A. Inui, Hydrogen-water enhances 5-fluorouracil-induced inhibition of colon cancer, *PeerJ* 3 (2015) e859.
- [10] Y. Jiang, G. Liu, L. Zhang, S. Cheng, C. Luo, Y. Liao, S. Guo, Therapeutic efficacy of hydrogen-rich saline alone and in combination with PI3K inhibitor in non-small cell lung cancer, *Mol. Med. Rep.* 18 (2) (2018) 2182–2190.
- [11] C. Zhang, D.-W. Zheng, C.-X. Li, M.-Z. Zou, W.-Y. Yu, M.-D. Liu, S.-Y. Peng, Z.-L. Zhong, X.-Z. Zhang, Hydrogen gas improves photothermal therapy of tumor and restrains the relapse of distant dormant tumor, *Biomaterials* 223 (2019) 119472.
- [12] K. Liu, J. Ou, S. Wang, J. Gao, L. Liu, Y. Ye, D.A. Wilson, Y. Hu, F. Peng, Y. Tu, Magnesium-based micromotors for enhanced active and synergistic hydrogen chemotherapy, *Appl. Mater. Today* 20 (2020) 100694.
- [13] J. Akagi, H. Baba, Hydrogen gas restores exhausted CD8+ T cells in patients with advanced colorectal cancer to improve prognosis, *Oncol. Rep.* 41 (1) (2019) 301–311.
- [14] K. Hayashida, M. Sano, I. Ohsawa, K. Shinmura, K. Tamaki, K. Kimura, J. Endo, T. Katayama, A. Kawamura, S. Kohsaka, S. Makino, S. Ohta, S. Ogawa, K. Fukuda, Inhalation of hydrogen gas reduces infarct size in the rat model of myocardial ischemia-reperfusion injury, *Biochem. Biophys. Res. Co.* 373 (1) (2008) 30–35.
- [15] Y. Zhang, Q. Sun, B. He, J. Xiao, Z. Wang, X. Sun, Anti-inflammatory effect of hydrogen-rich saline in a rat model of regional myocardial ischemia and reperfusion, *Int. J. Cardiol.* 148 (1) (2011) 91–95.
- [16] K. Nagatani, H. Nawashiro, S. Takeuchi, S. Tomura, N. Otani, H. Osada, K. Wada, H. Katoh, N. Tsuzuki, K. Mori, Safety of intravenous administration of hydrogen-enriched fluid in patients with acute cerebral ischemia: initial clinical studies, *Med. Gas Res.* 3 (1) (2013) 13.
- [17] Y. He, B. Zhang, Y. Chen, Q. Jin, J. Wu, F. Yan, H. Zheng, Image-guided hydrogen gas delivery for protection from myocardial ischemia-reperfusion injury via microbubbles, *ACS Appl. Mater. Interfaces* 9 (25) (2017) 21190–21199.
- [18] Z. Kou, P. Zhao, Z. Wang, Z. Jin, L. Chen, B.-L. Su, Q. He, Acid-responsive H₂-releasing Fe nanoparticles for safe and effective cancer therapy, *J. Mater. Chem. B* 7 (17) (2019) 2759–2765.
- [19] P. Zhao, Z. Jin, Q. Chen, T. Yang, D. Chen, J. Meng, X. Lu, Z. Gu, Q. He, Local generation of hydrogen for enhanced photothermal therapy, *Nat. Commun.* 9 (1) (2018) 4241.

- [20] M. Fan, Y. Wen, D. Ye, Z. Jin, P. Zhao, D. Chen, X. Lu, Q. He, Acid-responsive H₂-releasing 2D MgB₂ nanosheet for therapeutic synergy and side effect attenuation of gastric cancer chemotherapy, *Adv. Healthcare Mater.* (2019) 1900157, 0(0).
- [21] S. Thomas, N.V. Medhekar, G.S. Frankel, N. Birbilis, Corrosion mechanism and hydrogen evolution on Mg, *Curr. Opin. Solid St. M.* 19 (2) (2015) 85–94.
- [22] D. Zhao, S. Huang, F. Lu, B. Wang, L. Yang, L. Qin, K. Yang, Y. Li, W. Li, W. Wang, S. Tian, X. Zhang, W. Gao, Z. Wang, Y. Zhang, X. Xie, J. Wang, J. Li, Vascularized bone grafting fixed by biodegradable magnesium screw for treating osteonecrosis of the femoral head, *Biomaterials* 81 (2016) 84–92.
- [23] J.-W. Lee, H.-S. Han, K.-J. Han, J. Park, H. Jeon, M.-R. Ok, H.-K. Seok, J.-P. Ahn, K. E. Lee, D.-H. Lee, S.-J. Yang, S.-Y. Cho, P.-R. Cha, H. Kwon, T.-H. Nam, J.H.L. Han, H.-J. Rho, K.-S. Lee, Y.-C. Kim, D. Mantovani, Long-term clinical study and multiscale analysis of in vivo biodegradation mechanism of Mg alloy, *P. Natl. Acad. Sci. USA* 113 (3) (2016) 716.
- [24] D. Zhao, A. Brown, T. Wang, S. Yoshizawa, C. Sfeir, W.R. Heineman, In vivo quantification of hydrogen gas concentration in bone marrow surrounding magnesium fracture fixation hardware using an electrochemical hydrogen gas sensor, *Acta Biomater.* 73 (2018) 559–566.
- [25] M. Nan, C. Yangmei, Y. Bangcheng, Magnesium metal—a potential biomaterial with antibone cancer properties, *J. Biomed. Mater. Res. A* 102 (8) (2014) 2644–2651.
- [26] Y.M. Chen, M. Xiao, H. Zhao, B.C. Yang, On the antitumor properties of biomedical magnesium metal, *J. Mater. Chem. B* 3 (5) (2015) 849–858.
- [27] W.L. Wan, Y.J. Lin, P.C. Shih, Y.R. Bow, Q. Cui, Y. Chang, W.T. Chia, H.W. Sung, An InSitu depot for continuous evolution of gaseous H₂ mediated by a magnesium passivation/activation cycle for treating osteoarthritis, *Angew Chem. Int. Ed. Engl.* 57 (31) (2018) 9875–9879.
- [28] Z. Shi, A. Atrens, An innovative specimen configuration for the study of Mg corrosion, *Corrosion Sci.* 53 (1) (2011) 226–246.
- [29] R. Zan, W. Ji, S. Qiao, H. Wu, W. Wang, T. Ji, B. Yang, S. Zhang, C. Luo, Y. Song, J. Ni, X. Zhang, Biodegradable magnesium implants: a potential scaffold for bone tumor patients, *Sci. China Mater.* 64 (4) (2021) 1007–1020.
- [30] S. Qiao, Y. Wang, R. Zan, H. Wu, Y. Sun, H. Peng, R. Zhang, Y. Song, J. Ni, S. Zhang, X. Zhang, Biodegradable Mg implants suppress the growth of ovarian tumor, *ACS Biomater. Sci. Eng.* 6 (3) (2020) 1755–1763.
- [31] Molecular Signatures Database v7.2. <http://www.gsea-msigdb.org/gsea/msigdb/index.jsp>.
- [32] KEGG PATHWAY Database. <https://www.genome.jp/kegg/pathway.html>.
- [33] Gene Ontology Resource. <http://geneontology.org/>.
- [34] X.-M. Yuan, W. Li, H. Dalen, J. Lotem, R. Kama, L. Sachs, U.T. Brunk, Lysosomal destabilization in p53-induced apoptosis, *P. Natl. Acad. Sci. USA* 99 (9) (2002) 6286.
- [35] T. Kirkegaard, M. Jäättelä, Lysosomal involvement in cell death and cancer, *BBA-Mol. Cell Res.* 1793 (4) (2009) 746–754.
- [36] A.G. Porter, R.U. Jänicke, Emerging roles of caspase-3 in apoptosis, *Cell Death Differ.* 6 (2) (1999) 99–104.
- [37] Z.-H. Chen, H.C. Lam, Y. Jin, H.-P. Kim, J. Cao, S.-J. Lee, E. Ifedigbo, H. Parameswaran, S.W. Ryter, A.M.K. Choi, Autophagy protein microtubule-associated protein 1 light chain-3B (LC3B) activates extrinsic apoptosis during cigarette smoke-induced emphysema, *P. Natl. Acad. Sci. USA* 107 (44) (2010) 18880.
- [38] S. Yu, G. Li, P. Zhao, Q. Cheng, Q. He, D. Ma, W. Xue, NIR-Laser-Controlled hydrogen-releasing PdH nanohydride for synergistic hydrogen-photothermal antibacterial and wound-healing therapies, *Adv. Funct. Mater.* 29 (50) (2019) 1905697.
- [39] N.D. Marchenko, A. Zaika, U.M. Moll, Death signal-induced localization of p53 protein to mitochondria: a potential role IN apoptotic signaling^{*}, *J. Biol. Chem.* 275 (21) (2000) 16202–16212.
- [40] M. Mihara, S. Erster, A. Zaika, O. Petrenko, T. Chittenden, P. Pancoska, U.M. Moll, p53 has a direct apoptogenic role at the mitochondria, *Mol. Cell* 11 (3) (2003) 577–590.
- [41] J. Chen, The cell-cycle arrest and apoptotic functions of p53 in tumor initiation and progression, *Cold Spring Harb. Perspect. Med.* 6 (3) (2016) a026104, a026104.
- [42] M.R.A. Mowat, p53 in tumor progression: life, death, and everything, in: G. F. Vande Woude, G. Klein (Eds.), *Advances in Cancer Research*, Academic Press, 1998, pp. 25–48.